# REAL-TIME SYNCHRONOUS IMAGING OF ELECTROMECHANICAL RESONATOR MODE AND EQUILIBRIUM PROFILES

*Y. Linzon[1], D. Joe[1], R.A. Barton[1], R.B. Ilic[1], S. Krylov[2], J.M. Parpia[1], and H.G. Craighead[1]*
[1]Cornell University, Ithaca, NY, USA
[2]Tel Aviv University, Tel Aviv, ISRAEL

## ABSTRACT

The single-shot interferometric imaging of normal mode dynamics in MEMS resonators, oscillating in the radio frequency (rf) regime, is demonstrated by synchronous imaging with a pulsed nanosecond laser. Profiles of mechanical modes in suspended silicon and graphene thin-film structures, and their extracted equilibrium profiles, are measured through nondestructive all-optical Fabry-Perot reflectance fits to the temporal traces. As a proof of principle, the modal patterns of a microdrum silicon resonator is analyzed, and its extracted vibration modes and equilibrium profile show good agreement with other characterization and numerical estimations.

## INTRODUCTION

In MEMS and NEMS resonators, visualization of actuated vibration modes and equilibrium elevation profiles provide an important device characterization. We demonstrate the first application of synchronous imaging in the real-time estimation of MEMS- and NEMS-resonator actuation mode patterns and equilibrium profiles.

While scanning electron [1] and atomic-force [2] microscopes offer unrivaled spatial resolutions in imaging of resonator structures, they cannot yield sub-cycle time-resolved images of mechanical profiles during *in-situ* motion at radiofrequencies. In the realm of non-invasive optical characterization of MEMS and NEMS devices, several techniques are available, such as scanning interferometry [3] and laser Doppler vibrometry [4]. In previous methods, however, spatiotemporal characterization usually relies on scanning, and thus requires the use of slow translation stages and complex data analysis algorithms, sacrificing acquisition time for high spatial resolution and amplitude sensitivities. In this work we demonstrated real-time synchronous imaging of electromechanical mode patterns and profiles. This is realized by direct pulsing of a nanosecond wide-field imaging laser which is synchronized with electrical drive. Temporal resolutions are attained by sweeping the locked phase difference between the drive and imaging beam signals.

## EXPERIMENTAL SETUP

Figure 1 illustrates our setup, in which the resonator resides in a vacuum chamber (P~4×10^{-2} Torr) with a front optical window and backside electrical feed-through.

In a frequency-domain scan (FDS) arm [Fig. 1(a)], the resonator is electrostatically driven by a swept rf network analyzer. The drive signal is amplified and subsequently dc-biased through an rf-bias-tee in order to maximize the mechanical amplitude and the associated interference depths of the reflected optical waves. A continuous-wave (cw) laser diode (at wavelength 633 nm) is focused by a long working distance objective lens (×20) onto the resonator, the substrate under which is reflective. Polarization beam splitters (PBS) collect and focus the back-reflected beam onto a low-noise sensitive detector, which closes a return-loop with the analyzer. In the analyzer, the rf-modulated signal is filtered and the spectral response is measured. This corresponds to the Fabry-Perot interferences matching each scanned drive frequency. In order to avoid laser-induced artifacts that are not purely mechanical, minimum spot fluence (< 0.2 mW/μm^{-2}) are used. We use this arm for sensitive identification of steady-state resonant MEMS modes. Modes in the range 40 kHz-3 GHz can be observed, as limited by the analyzer.

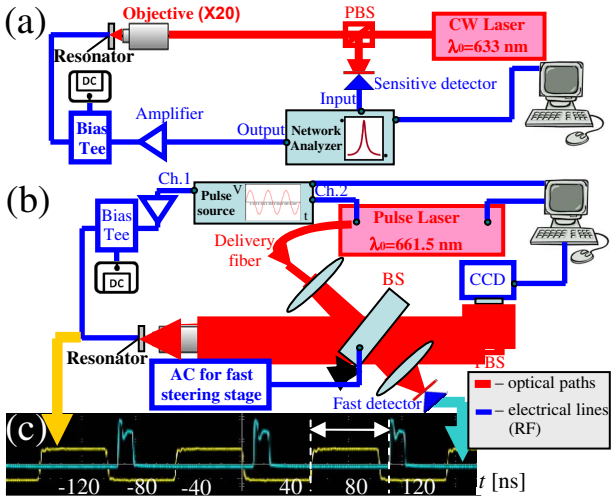


*Figure 1: Experimental setup to study MEMS/NEMS resonators: (a) Frequency-domain arm, consisting of a sweeping rf network analyzer and a cw optical return loop. (b) Time-domain synchronous imaging arm. (c) A typical oscilloscope temporal trace of electrical drive (50% duty cycle) and imaging beam pulses (10% duty cycle).*

In the synchronous arm [Fig. 1(b)], a fiber-delivered pulse laser beam (Toptica iPulse at wavelength 661.5 nm) is used for wide-field resonator visualization. Direct electrical modulation with nanosecond gating times with minimum optical and temporal distortion is possible in the theoretical spectral range 0-500 MHz, but practically only in the range 0-200 MHz a good modulation depth is observed. This beam is collimated and illuminates the resonator through the reflections from a beam-splitter (BS). The same objective as

in the FDS arm is used for full-aperture illumination of the resonator. The frequency is set at a resonant mode (known from the FDS arm measurement, or located by manual probing of the imaging frequency), and all drives are supplied through the outputs of a phase-locked dual channel electrical pulse source producing unipolar square waves. One channel is used for the drive, with a duty cycle of 50%, whereas the second channel triggers the imaging beam with narrow pulses of duty cycle 10% [Fig. 1(c) shows a typical oscilloscope trace of the drive and imaging pulse trains]. This provides an effective temporal window of 0.1$T$, where $T$ is the period. The stationary phase difference $\Delta\phi$ is scanned and corresponds to the mechanical inter-cycle sampling time $\Delta T$. The BS is mounted on a fast-steering stage to average the arbitrary speckle-patterns, which are typically observed when collimated laser beams are used in nonuniform surface imaging. The back-reflected signal is focused on a standard 3 megapixel CCD camera at the objective imaging plane. Direct optical synchronization obviates scanning mechanical stages, except for the above-mentioned steering BS. The high peak powers available (110 mW at the delivery fiber output without modulation) are crucial for sufficient back-reflection imaging signal, and substantial power losses are experienced at the BS interfaces. Higher duty cycle levels increase the power available for imaging on account of reduced temporal resolutions.

## RESULTS AND ANALYSIS

In Figs. 2 and 3 we analyze here a circularly symmetric polycrystalline-Si (PolySi, refractive index: $n$=3.8) microdrum resonator (disk shaped film of diameter 25 µm and a thickness of ~330 nm, suspended over an air-gap on top of a [1 0 0]-Si wafer, where the latter serves as an actuation electrode. An orifice (wet-etch hole), which is 4 µm in diameter is present at the drum center. Figure 2(a) shows an FDS spectrum of the drum [using arm 1(a)] under a 2 dBm (280 mV) ac excitation and a 22 V applied dc bias. Mostly the first two axi-symmetric modes [(0,1) and (0,2), indexed by the number of nodes in the (circumferential, radial) directions] are efficiently excited. Synchronous images [using arm 1(b)] at different times within a cycle, $0<\Delta\phi<360°$, are shown for the fundamental (0,1) and second symmetric (0,2) modes in Figs. 2(b) and 2(c), respectively. All differential interference images in Fig. 2 were obtained with respect to the reference image (bottom left of Fig. 2, full contrast) in the absence of electromechanical drive. Each image is subtracted from the reference and normalized by it. The modal patterns are observed in real-time as a function of phase through the stationary image at the camera. As suggested by the contrast variations, in this resonator, the actuation regime is close to an optical fringe minimum at the imaging wavelength.

To extract from the measured optical images the actual mechanical mode shapes and device equilibrium suspensions, we use Fabry-Perot interference analysis of the temporal traces. Figure 3 illustrates the cross-section of our resonator, consisting of three dielectric layers (polySi, air gap, and thick single-crystal Si substrate), and definitions of model parameters. We write the air gap displacement as $d_1(x,t) = d_0 + A\cos(\omega t + \phi_0)$, where $(A, d_0, \phi_0)$ are the fitting parameters, $\omega$ is the drive frequency (assuming a linear temporal response) and $t$ is the time. At each in-plane radial point $x$, $A(x)$ corresponds to the vibration amplitude, $d_0(x)$ to the air-gap elevation, and $\phi_0(x)$ to the phase between electrical drive and optical pulses.

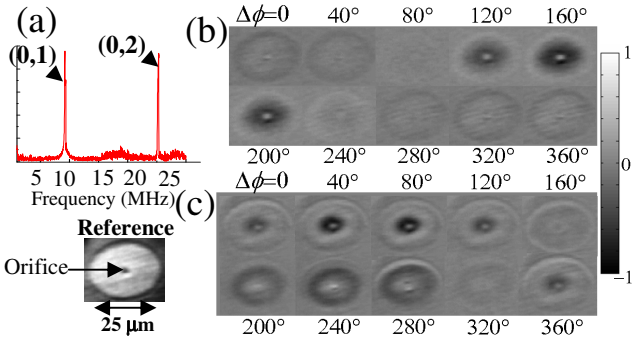


*Figure 2: Drum resonator modes. (a) FDS spectrum. (b),(c) Synchronous imaging within a single mechanical cycle for: (b) fundamental mode **(0,1)**, f=9.2 MHz, and (c) second symmetric mode **(0,2)**, f=25.5 MHz. All interference images are subtracted from the full contrast reference image of the drum (bottom left) and normalized.*

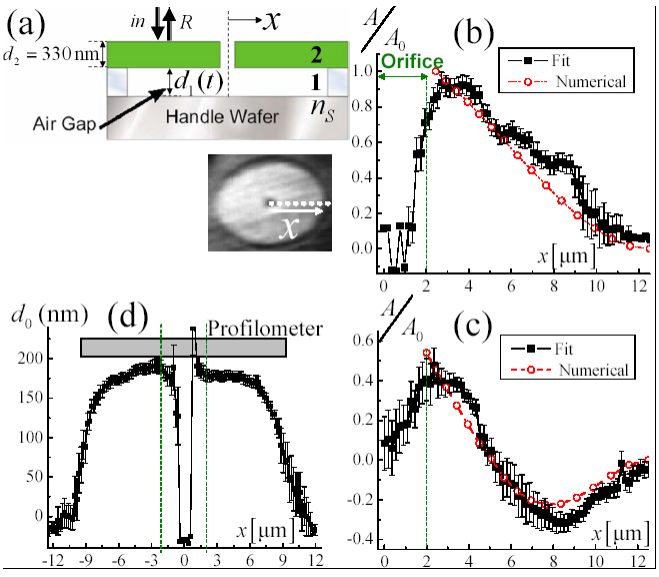


*Figure 3: (a) Cross-section geometry used in the analysis. (b),(c) Mode profiles [as estimated along the dashed line in the inset of (a)] for the first (0,1) and second (0,2) modes, respectively. (d) Equilibrium profile ($d_0$) estimated from the first mode fit. Hollow circles indicate the numerical profile estimations for this device. Error bars in the data indicate the nonlinear least-square fit boundaries within a 95% confidence level around the averaged values.*

Using a multilayer-film interference analysis [5] and assuming normal incidence (which are valid as a good approximation in the adopted low grazing-angle illumination of the resonator), the reflection coefficient is computed from:

$$\begin{pmatrix} a \\ b \end{pmatrix} = M_{tot.} \begin{pmatrix} 1 \\ n_s \end{pmatrix} \qquad (1)$$

where $a$ and $b$ are scalars, $M_{tot.} = M_2 M_1(t)$ is the composite transfer matrix [5] and $n_s$ is the substrate refractive index. The corresponding reflectance is then $R = |(a-b)/(a+b)|^2$, and the measured differential intensity corresponds to $I_{diff.}(x,t) = R[x, d_1(t)] - R[x, d_0]$. A fit is performed independently in each point $x$ on a radial cross section of the drum [inset of Fig. 3(a)]. The mode profiles extracted for this section are shown for the (0,1) and (0,2) modes in Figs. 3(b) and 3(c), respectively. The equilibrium elevation profile $d_0(x)$ extracted from the first mode data is shown in Fig. 3(d). All profiles in the drum region converge within a small number of iterations (<1000 in these scans) and usually yield smooth, low-error profiles along a resonator section, provided that a sufficient signal-to-noise is available for the temporal traces in the images.

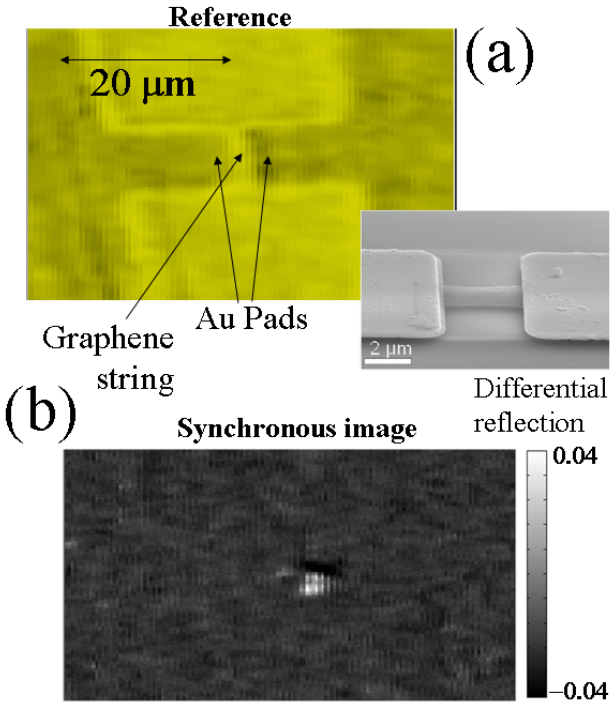


*Figure 4: Graphene NEMS string deposited on gold pads and driven electrically via the right electrode. (a) Reference image. The inset shows a scanning electron microscope image of the device. (b) Synchronous image of the averaged mechanical mode (bottom), at 25.4 MHz.*

Numerical finite-element simulations [6] of the resonator modes, using a circumferentially clamped 25 μm drum with a concentric hole of 4 μm diameter, 190 nm elevation of the film center above the clamped ends, and a cross-section geometry as in Fig. 3(a), reveal good correspondence with the experimental results in terms of the mode profiles [hollow circles in Fig. 3] and the fundamental mode frequency [Fig. 2(a)]. Small deviations of the measured profile shapes and mode frequencies from the ideal numerical values are estimated to result from the presence of residual stress in the film, dc-bias induced nonlinear interactions, and device imperfections. Independent static profilometry characterization around the orifice region (without vacuum or actuation) yielded a thickness of 200-225 nm for the air gap in this device [gray area in Fig. 3(d)], in agreement with our all-optical estimations for $d_0(x)$ near the drum center.

The synchronous imaging technique is also applicable in a host of other device geometries and compositions. In Fig. 4, the interferometric image of a single atomic layer graphene NEMS resonator fundamental mode, as well as its supporting gold electrode mode (the pad of which is undercut near the string, see the inset of Fig. 4), is shown as imaged and averaged over half a cycle of the actuation frequency (25.4 MHz). Note that even though the graphene string cannot be resolved in the reference image (due to its dimensions being comparable with the laser wavelength, and its low index of refraction, see inset of Fig. 4), it can be discerned in the synchronous mode image and separated from the drive pad mode, which is oscillating at the same frequency under these conditions. The anti-phase oscillation of the metal and graphene modes, are known as "avoided crossing" in such devices [7] and are typically observed in intersections between metal and graphene modes with enhanced mechanical response of the string, corresponding to large energy transfer from the pad in resonance.

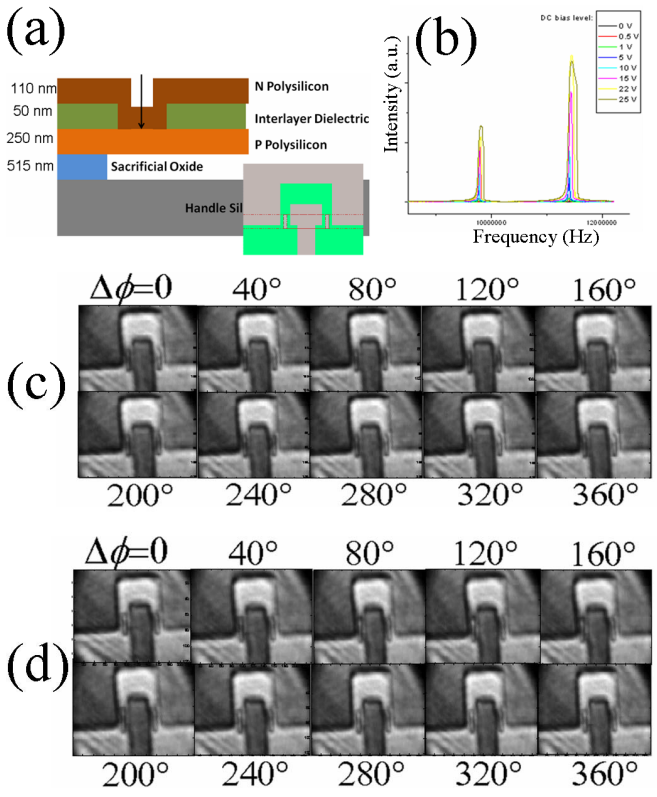


*Figure 5: (a) Cross-section geometry (inset: top view) of a multi-layer cantilever device, and (b) its corresponding FDS spectrum. (c) Synchronous imaging of low (f=9.8 MHz) and high (f=11.5 MHz) vibration modes, without background subtraction.*

Figure 5 shows the spatiotemporal interference imaging of the vibration modes in a more complicated multi-layer cantilever device (cross section and top-view geometries depicted in Fig. 5(a), and FDS spectrum shown in Fig. 5(b)). Here the two modes, belonging to actuation of different sides of the composite cantilever, can be easily and quickly identified from the synchronous images of the corresponding frequencies (Figs. 5(c) and 5(d)).

## CONCLUSIONS

The technique of real-time synchronous imaging provides rapid and robust spatiotemporal visualization and characterization of *in-situ* electromechanical modes at radiofrequencies. This includes various silicon-based MEMS resonators (Figs. 2,3), and NEMS resonators such as thin as single layer graphene sheets (Fig. 4), where direct single-shot discrimination between various components, resonating at the same frequency, is possible. The sensitivity of amplitude detection in the polySi on Si devices, deduced from Figs. 3(b) and 3(c) were 10%-30% of the peak amplitude (estimated to be ~120 nm in the above conditions). We note, however, that the sensitivity is significantly enhanced in devices which operate near more sensitive regimes of the optical reflectance, and when the duty cycle of the imaging beam is increased (as in Fig. 4, where the graphene string peak amplitude was estimated to be ~100 picometer).

## REFERENCES

[1] C. Ke and H. D. Espinosa, "In Situ Electron Microscopy Electromechanical Characterization of a Bistable NEMS Device", *Small*, vol. 2, (2006), pp. 1484-1489.

[2] B. Ilic, S. Krylov, L.M. Bellan, and H.G. Craighead, "Dynamic characterization of nanoelectromechanical oscillators by atomic force microscopy", *J. Appl. Phys.*, vol. 101, (2007), pp. 044308.

[3] C. Rembe and R. S. Muller, "Measurement System for Full Three-Dimensional Motion Characterization of MEMS", *J. Microelectromech. Syst.*, vol. 11 (2002), pp. 479-488.

[4] P. Castellini, M. Martarelli, and E.P. Tomasini, "Laser Doppler Vibrometry: Development of advanced solutions answering to technology's needs", *Mech. Syst. Signal Process.*, vol. 20 (2006), pp. 1265-1285.

[5] M. Bass, *Handbook of Optics* (McGraw-Hill, 1995).

[6] K.J. Bathe, *Automatic Dynamic Incremental Nonlinear Analysis* (ADINA R&D, Inc., 2005).

[7] C. Chen, S. Rosenblatt, K.I. Bolotin, W. Kalb, P. Kim, I. Kymissis, H.L. Stormer, T.F. Heinz, and J. Hone, "Performance of monolayer graphene nanomechanical resonators with electrical readout", *Nature Nanotechnology*, vol. 4 (2009), pp. 861-867.